GABA and glutamate moderate beta-amyloid related functional connectivity in cognitively unimpaired old-aged adults

F.C. Quevenco[a,1], S.J. Schreiner[a,b,1], M.G. Preti[f,g], J.M.G. van Bergen[a], T. Kirchner[c], M. Wyss[c], S.C. Steininger[a,b], A. Gietl[a], S.E. Leh[a,b], A. Buck[d], K.P. Pruessmann[c,h], C. Hock[a,b,h], R.M. Nitsch[a,b,h], A. Henning[c,e], D. Van De Ville[f,g], P.G. Unschuld[a,b,h,*]

[a] Institute for Regenerative Medicine (IREM), University of Zurich, Zurich, Switzerland
[b] Hospital for Psychogeriatric Medicine, Psychiatric University Hospital Zurich (PUK), Zurich, Switzerland
[c] Institute for Biomedical Engineering, University of Zurich and ETH Zurich, Zurich, Switzerland
[d] Division of Nuclear Medicine, University Hospital Zurich (USZ), Zurich, Switzerland
[e] Max Planck Institute for Biological Cybernetics, Tubingen, Germany
[f] Department of Radiology and Medical Informatics, Université de Genève, Switzerland
[g] Institute of Bioengineering, École polytechnique fédérale de Lausanne, Switzerland
[h] Neuroscience Center Zurich (ZNZ), Zurich, Switzerland

ARTICLE INFO

ABSTRACT

Background: Effects of beta-amyloid accumulation on neuronal function precede the clinical manifestation of Alzheimer's disease (AD) by years and affect distinct cognitive brain networks. As previous studies suggest a link between beta-amyloid and dysregulation of excitatory and inhibitory neurotransmitters, we aimed to investigate the impact of GABA and glutamate on beta-amyloid related functional connectivity.
Methods: 29 cognitively unimpaired old-aged adults (age = 70.03 ± 5.77 years) were administered 11C-Pittsburgh Compound B (PiB) positron-emission tomography (PET), and MRI at 7 Tesla (7T) including blood oxygen level dependent (BOLD) functional MRI (fMRI) at rest for measuring static and dynamic functional connectivity. An advanced 7T MR spectroscopic imaging (MRSI) sequence based on the free induction decay acquisition localized by outer volume suppression' (FIDLOVS) technology was used for gray matter specific measures of GABA and glutamate in the posterior cingulate and precuneus (PCP) region.
Results: GABA and glutamate MR-spectra indicated significantly higher levels in gray matter than in white matter. A global effect of beta-amyloid on functional connectivity in the frontal, occipital and inferior temporal lobes was observable. Interactive effects of beta-amyloid with gray matter GABA displayed positive PCP connectivity to the frontomedial regions, and the interaction of beta-amyloid with gray matter glutamate indicated positive PCP connectivity to frontal and cerebellar regions. Furthermore, decreased whole-brain but increased fronto-occipital and temporo-parietal dynamic connectivity was found, when GABA interacted with regional beta-amyloid deposits in the amygdala, frontal lobe, hippocampus, insula and striatum.
Conclusions: GABA, and less so glutamate, may moderate beta-amyloid related functional connectivity. Additional research is needed to better characterize their interaction and potential impact on AD.

1. Introduction

Coherent brain network activity is an indicator of healthy brain functioning and depends on a balanced interplay between inhibitory and excitatory neuronal activity (Ferreira and Busatto, 2013; Fox and Raichle, 2007; Seeley, 2017; van den Heuvel et al., 2009). Neurodegenerative diseases are characterized by an aggregation of various pathological proteins (Robinson et al., 2018) that is associated with compromised coordination of neuronal brain activity (Brettschneider et al., 2015; Jagust and Mormino, 2011). Alzheimer's disease (AD) is the most frequent cause for neurodegenerative dementia at high age and is characterized by a decade long preclinical phase during which beta-amyloid pathology manifests, while cognitive performance remains normal for a long time (Dubois et al., 2016; Sperling et al., 2011).

Moreover, the presence of beta-amyloid in AD risk-populations is associated with distinct changes in brain network activity, as indicated by altered patterns of synchronous neural activity of functionally connected brain regions (Franzmeier et al., 2017; Mormino et al., 2011; Sepulcre et al., 2017; Sorg et al., 2007; Steininger et al., 2014; Teipel et al., 2016b). Interestingly, beta-amyloid related connectivity changes particularly affect intrinsic cognitive networks such as the default mode network (DMN) (Buckner et al., 2009; Hedden et al., 2009; Sheline et al., 2010). A characteristic feature of intrinsic networks such as the DMN is that they are constituted by distinct sets of functionally connected 'hubs' that synchronously activate at rest (Buckner et al., 2008; Greicius et al., 2003; Raichle et al., 2001). Activity of intrinsic brain networks may be inferred on by measuring 'static' connectivity of neuronal tissue to a major network hub using blood oxygen level dependent (BOLD) functional magnetic resonance imaging (fMRI) at rest (Friston et al., 1993). More recently, also approaches for measuring 'dynamic' connectivity have been established that allow for the variability of functional connectivity within networks over time (Chang and Glover, 2010; Handwerker et al., 2012; Hutchison et al., 2013; Preti et al., 2017).

The posterior cingulate and precuneus (PCP) region is a major 'hub' in various intrinsic brain networks, and pathological change pertaining to the PCP is a robust finding in preclinical AD (Esposito et al., 2013; Lustig et al., 2003; Sheline et al., 2010; Teipel et al., 2016a). Moreover, as the PCP plays a central role for episodic memory processing, this is consistent with episodic memory typically being first affected when cognitive impairment manifests in the course of AD (Albert et al., 2011; Cieri and Esposito, 2018).

GABA and glutamate represent major excitatory and inhibitory neurotransmitters in the human central nervous system. A concatenation of preclinical studies suggest that beta-amyloid aggregation is linked to local dysfunction of neuronal inhibition and excitation (Bero et al., 2011; Busche et al., 2008; Palop et al., 2007; Ulrich, 2015). However, to our knowledge, the interaction between GABA, glutamate and beta-amyloid has not been investigated in human in vivo study populations yet.

Allowing for these earlier findings that suggest an intimate relationship between beta-amyloid and both regulation of neuronal inhibition and excitation, we hypothesized that the impact of pathological beta-amyloid on intrinsic brain network activity is moderated by GABA and glutamate. Thus, aims of the current study were: (1) to determine presence and activity of intrinsic beta-amyloid associated brain networks in cognitively unimpaired old-aged adults at rest; (2) to establish whether Glutamate and GABA moderate effects of beta-amyloid on network activity.

To this effect, GABA and glutamate were specifically assessed in gray and also white matter of the PCP using magnetic resonance spectroscopic imaging (MRSI) based on the 'free induction decay acquisition localized by outer volume suppression' (FIDLOVS) methodology (Henning et al., 2009) at ultra-high field strength of 7 Tesla (7 T) for increased spatial resolution of spectral information and increased signal-to-noise ratio (SNR). Beta-amyloid plaque density was assessed by 11C-Pittsburgh-Compound B (PiB) positron emission tomography (PET) (Klunk et al., 2004). 'Static' functional connectivity was measured using the PCP as a seed for BOLD synchronicity at rest (Whitfield-Gabrieli and Nieto-Castanon, 2012). In addition, whole-brain 'dynamic' connectivity was assessed as a measure of the temporal dynamics of BOLD synchronicity patterns (Allen et al., 2014) by applying a sliding time window approach (Leonardi et al., 2013; Richiardi et al., 2012).

2. Materials and methods

2.1. Study population

The study sample included a total of 29 (17 males, 12 females) cognitively unimpaired old-aged adults (mean age:

Table 1

Demographics of the sample population. The last column contains p-values of two-sample *t*-tests to ensure there are no significant demographic differences between the GABA and Glutamate sample.

	All	GABA	Glutamate	p-values
N total	29	24	28	N/A
Age	70.03 ± 5.77	69.54 ± 5.76	69.43 ± 5.37	0.91
Males	17	14	17	0.86
ApoE-e4	8	7	7	0.74
MMSE	29.41 ± 0.81	29.46 ± 0.85	29.48 ± 0.82	0.88
BMI	25.62 ± 3.77	24.95 ± 2.99	25.44 ± 3.78	0.57
Education (in years)	15.83 ± 2.48	16.00 ± 2.54	15.79 ± 2.38	0.88
Cortical PiB Ratio	1.25 ± 0.34	1.22 ± 0.29	1.21 ± 0.27	0.93
PiB +	3	2	2	N/A

69.75 ± 5.57 years), who where recruited from an ongoing cohort study of ours (Gietl et al., 2015; Schreiner et al., 2014; Steininger et al., 2014). Due to missing MRSI data, not all 29 participants were included in the subsequent combined connectivity analyses (see Table 1). To ensure normal cognitive performance, potential study participants were cognitively evaluated by applying a battery of neuropsychological tests as indicated earlier (Quevenco et al., 2017b). These included the Mini-mental State Examination (MMSE) (Folstein et al., 1975) as a screening test for present cognitive impairment. For detection of isolated neuropsychological deficits in potential study participants, additionally the Revised Boston Naming Test (BNT) (Nicholas et al., 1988), Digit Spans Backward (Gregoire and Van der Linden, 1997), Trail Making Test (TMT) B/A (Tombaugh, 2004); Verbal Learning And Memory Test (VLMT): delayed recall (Lange et al., 2002) were performed. Exclusion criteria were: any present medication that may affect cognition, general magnetic resonance imaging (MRI) exclusion criteria, contraindications against venipuncture, clinically relevant changes in red blood cell count, any acute severe medical, neurological or psychiatric condition, present or past drug abuse, allergy to the PET tracer 11C-PiB, significant earlier exposure to radiation. Moreover, any participant who showed MRI evidence of infarction, focal or significant hemorrhagic lesions, was excluded from this study. The Apolipoprotein E ε4 allele was assessed to detect possible overrepresentation of genetic risk for AD and brain amyloidosis in the investigated sample (Corder et al., 1993; Kantarci et al., 2012). All study procedures were carried out in accordance with regulatory requirements (Kantonale Ethikkommission Zürich, www.kek.zh.ch) and the Declaration of Helsinki. Written informed consent was obtained from all candidates prior to participation in thi study.

2.2. Acquisition of MRI data

All participants underwent a single scanning session in a Philips Achieva 7-Tesla (7 T) whole-body scanner (Philips Healthcare, Best, The Netherlands) equipped with a Nova Medical quadrature transmit head coil and a 32-channel receive coil array. High-resolution T1-weighted 3D-MPRAGE structural images (repetition time (TR)/echo time (TE) = 8.22 ms/3.74 ms, voxel size = 0.86 × 0.86, scan duration = 653.71 s, slice thickness = 0.9 mm, flip angle = 7°, FOV = 220 × 157.5 × 198.36) were obtained for referencing, automated multi-channel image segmentation, and localization of the volumes of interest (VOIs) for magnetic resonance spectroscopic imaging (MRSI), as done in earlier studies of ours (Schreiner et al., 2018; Schreiner et al., 2016). In brief, we acquired a refined high-resolution direct free-induction-decay (FID) sequence (acquisition delay = 2.5 ms, TR = 644 ms, in-plane resolution = 3.5 × 3.5 mm2, slice thickness = 12 mm, scan duration = 1762s) based on "FID acquisition, localized by outer volume suppression" (FIDLOVS) (Henning et al., 2009), with water suppression similar to variable power RF pulses with optimized relaxation delays (VAPOR) (Tkac et al., 1999), but without outer

volume or fat suppression (Bogner et al., 2012). Dynamic B0 shimming was conducted to reduce magnetic field inhomogeneities particularly due to the absence of outer volume or fat suppression (Fillmer et al., 2015). To obtain the exact anatomical reference of these images, a T1-weighted structural turbo spin echo (TSE) image (TR/TE = 5.7 ms/ 2.9 ms, resolution = $0.9 \times 0.9 \times 1.5$ mm) was acquired using the same FOV dimensions as the MRSI slab. Resting-state fMRI data for each subject was acquired using an echo planar imaging (EPI) sequence (TR = 2500 ms, slice thickness = 3 mm, flip angle = 45°, voxel size = 1.719×1.719 mm, scan duration = 537.5 s, number of slices = 50, FOV = 220x150x220mm).

2.3. Defining the posterior cingulate/Precuneus (PCP) slab for metabolite measurement

To assess MRSI metabolites in the Posterior Cingulate/Precuneus (PCP), the Hammers atlas, a 3-dimensional maximum probability atlas of the human brain containing 83 anatomical labels (Gousias et al., 2008; Hammers et al., 2003), was modified in-house to generate a binary mask of the PCP. This ROI comprised the PCP, corresponding to the Brodmann areas BA 31 and the medial parts of BA 7. The superior and inferior anatomical borders were defined by the extent of the MRSI slab in the z direction, the rostral border by the posterior part of the Anterior Cingulate cortex, and the posterior border by the Postero-occipital fissure. Custom ROIs were acquired using a pipeline applied to the anatomical ROIs of the PCP per subject (Schreiner et al., 2016).

2.4. Acquisition of PET data

Cortical beta-amyloid deposits were measured using Positron Emission Tomography (PET) with the tracer 11-C Pittsburgh Compound B (PiB) (Klunk et al., 2004). Participants were intravenously administered a dose of approximately 350 MBq of the tracer and amyloid deposition was estimated based on late frame signals representing 50–70 min post-injection. Measures of cerebral beta-amyloid load per subject was derived from the ratio of standardized uptake values (SUV) of cortical PiB-VOIs, referenced to cerebellar gray matter SUV after co-registration using the PMOD brain tool (PNEURO) software, Version 3.4 (PMOD Technologies Ltd., Zurich, Switzerland) as described in our previous studies (Schreiner et al., 2016; Steininger et al., 2014). Standardized PiB-SUV were used to calculate cortical to cerebellar PiB retention ratio units ("cortical-PiB") (Jack et al., 2009), and to determine "amyloid-positive" status using an earlier defined threshold of ours (Gietl et al., 2015).

2.5. Processing of magnetic resonance spectroscopic imaging (MRSI) data

The post-processing pipeline of MRSI data conducted, is identical to the pipeline used in an earlier publication (Schreiner et al., 2016). Tissue-specific anatomical sub-regions of PCP were defined on the MRSI slab that covered the PCP region. GABA and glutamate, referenced to Creatine, were estimated with LC model (Provencher, 2001) from averaged MRSI spectra from PCP gray matter and white matter separately.

Sufficient MRSI quality was determined by visual inspection of all spectra (Fig. 1), as conducted in previous studies (Schreiner et al., 2018; Schreiner et al., 2016) and applying recommended cut-offs for SNR (Oz G, Alger JR, Barker PB, et al. Clinical proton MR spectroscopy in central nervous system disorders. Radiology. 2014 Mar;270(3):658-79). Further, we only considered spectra with relative Cramér-Rao Lower Bounds (CRLB) < 30%, despite the common practice of using relative CRLB < 20%. We chose this more liberal threshold, as a strict usage of relative CRLB may introduce bias by underestimating changes in metabolites with low levels (Kreis, 2016), e.g. GABA.

2.6. Processing of fMRI data and assessment of dynamic functional connectivity

Structural and functional images were preprocessed using a standardized in-house developed pipeline (Richiardi et al., 2012). This pipeline was implemented with MATLAB scripts (MATLAB 2015b, Version 8.6, MathWorks Inc., Natick, MA, USA), including functions from SPM8 and SPM12 (www.fil.ion.ucl.uk/spm) and DPARSFA toolboxes (Chao-Gan and Yu-Feng, 2010). Preprocessing parameters used in this study are identical to those used in an earlier dynamic functional connectivity study (Quevenco et al., 2017b). The images were spatially realigned and smoothed and nuisance variables were regressed out from the regional time series. The functional volumes were then regionally parcellated using the automated anatomical labelling (AAL) atlas. Regional mean time series were extracted by averaging the preprocessed BOLD signal over all voxels in each region.

A sliding time window approach was used (window size: 24TRs (= 60s), step: 1TR (= 2.5 s)) to calculate the time-varying correlations between BOLD fluctuations in distinct brain regions. PCA was then used to extract meaningful connectivity patterns ('eigenconnectivities') that best capture dynamic functional connectivity (Quevenco et al., 2017b). These patterns are characterized by two main configurations: positive/red connections denote an increase in connectivity between a set of nodes, whereas negative/blue illustrate decreased connectivity between a given set of nodes.

The weighted time contributions of each eigenconnectivity (network) were calculated by projecting dynamic functional connectivity on a select number of eigenconnectivities. An eigenconnectivity number of 10 was sufficient to explain 37% of data variance when taking the diagonal of the decomposed PCA matrix, as indicated in previous studies of ours (Leonardi et al., 2013; Quevenco et al., 2017a). The measure assessed according to our predictor variables was the *percentage of positive weights* of each eigenconnectivity, which illustrates the propensity of an eigenconnectivity's preference towards increased connectivity between the red nodes and less connectivity between the blue nodes. Network signs (positive or negative) are thus used to illustrate alternations between: (1) increased connectivity (positive/red connections); and (2) decreased connectivity (negative/blue connections) between a set of nodes. Percentage of positive weights represents the amount of time a network contributes with a positive sign. A positive sign weight indicates a preference for a network to contribute to the dynamic functional connectivity in the first configuration (increased connectivity), whilst a negative sign weight indicates a preference for an eigenconnectivity to contribute in the second configuration (decreased connectivity).

Multimodal neuroimaging approach of combined 7 T FIDLOVS MRI (gray matter GABA and glutamate), 11C PiB-PET (beta-amyloid burden) and 7 T BOLD fMRI at rest (static and dynamic functional connectivity).

2.7. Statistical tests

All statistical tests were carried out using MATLAB (2015b, Version 8.6), the Statistics and Machine Learning Toolbox (Version 10.0) and the CONN toolbox (Whitfield-Gabrieli and Nieto-Castanon, 2012). Static functional connectivity changes in the context of cortical beta-amyloid and GABA and Glutamate levels in the PCP were assessed using the CONN toolbox with the MRSI PCP slab as a seed. Thus, any connectivity changes observed would regionally overlap with regions, where GABA and glutamate measures are obtained. Altered connectivity between identified regional clusters and the PCP were compared by post-hoc tests using CONN. R^2 values were obtained to investigate the degree of correlation between BOLD fluctuations of these clusters and the PCP.

Since the obtained PiB-load and metabolite measures are continuous variables, correlations between predictors and time contribution and
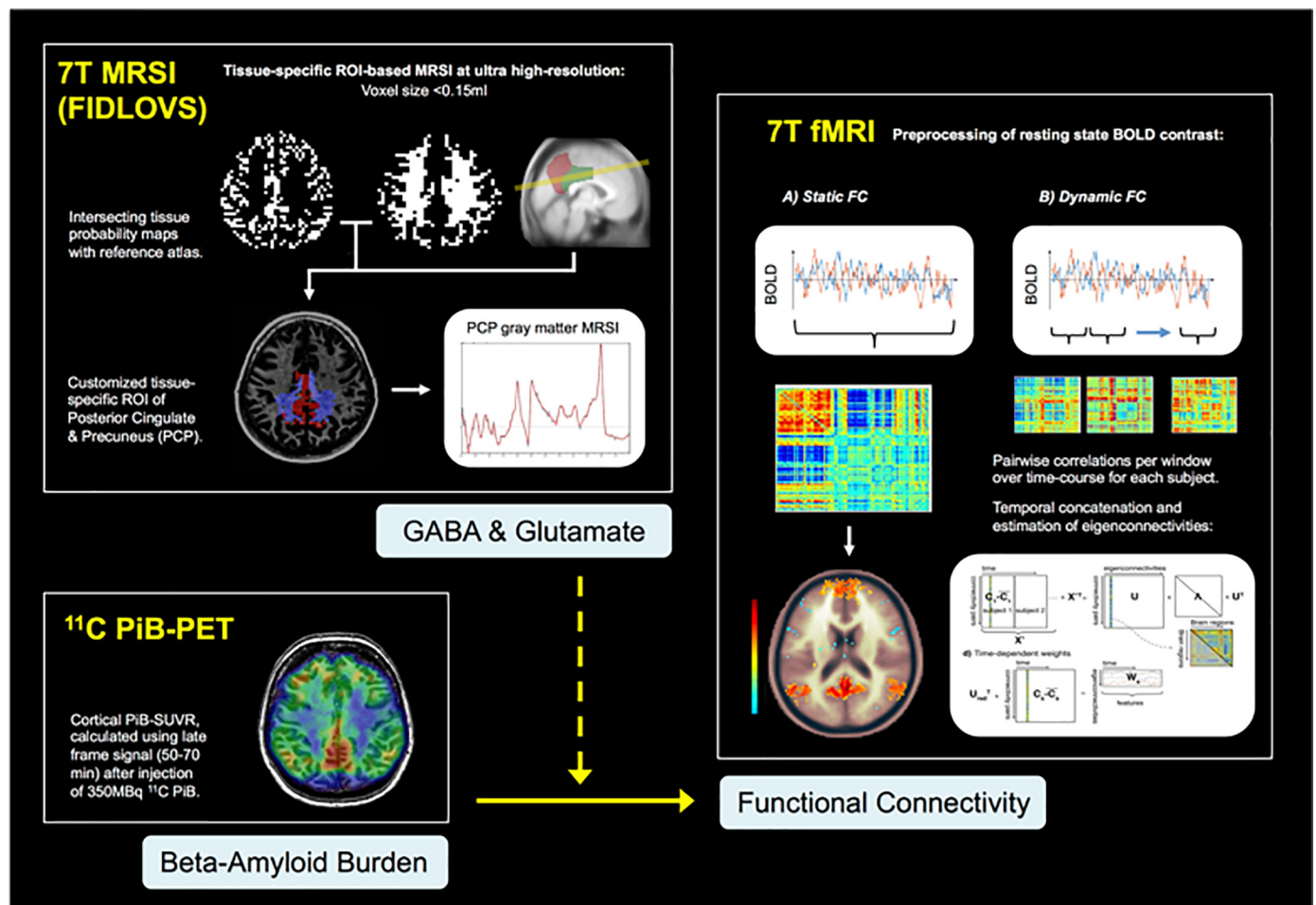
Fig. 1. Image processing and analysis workflow of PET, MRSI and fMRI data.

percentage positive weights of the dynamic functional connectivity were explored. A Canonical Correlation Analysis (CCA) was conducted to investigate any interaction effects of beta-amyloid with GABA and glutamate on dynamic functional connectivity measures. Statistical tests were all corrected for multiple comparisons using False Discovery Rate (FDR) correction according to the Benjamini-Hochberg procedure (Benjamini and Hochberg, 1995). This was done by obtaining the Benjamini-Hochberg critical values for each *p*-value based on the formula $(i/m)Q$, where i denotes the individual p-value's rank, m is the number of tests and Q represents the false discovery rate (0.05). The original values were then compared to the critical B—H values and the largest p value that has $p < (i/m)Q$ is significant and all the *p*-values smaller than it are also considered significant. Fig. 1 illustrates the image processing and workflow of all related statistical analyses.

3. Results

3.1. Sample population

Due to missing data or insufficient MRSI quality, 5 participants were excluded from the GABA analysis and 1 participant from the Glutamate analysis (see Table 1). In the remaining spectra, SNR was 14.2 + 4.8 in PCP GM and 13.0 ± 4.7 in PCP WM, respectively. Relative CRLB for GABA and Glutamate was 10.4 ± 4.0% and 4.3 ± 2.6% in GM, and 16.0 ± 7.0% and 5.8 ± 3.2% in WM, respectively. Neuropsychological testing indicated normal cognitive performance, as reflected by high group scores in the MMSE (29.41 ± 0.81). The study population included 8 APOE4 carriers, and 3 amyloid-positive participants (Fig. 2).

A: Axial representation of the Posterior Cingulate/Precuneus (PCP) gray matter (red) and white matter (blue) regions used for the MRSI analysis. Exemplary spectra analyzed using the LC Model to estimate average metabolite-levels between the gray (B) and white (C) matter. The colored lines denote the spectral fit and the black lines denote the residuals. Arrows mark the peaks for Glutamate (dashed) and GABA (solid). D: GABA and glutamate levels (each referenced to creatine) where higher in PCP gray matter (GM) compared to white matter (WM) (GABA: $t(45) = 2.26$, $p = 0.029$; Glutamate: $t(50) = 4.24$, $p < 0.001$). The asterisk indicates significance at $p < 0.05$.

3.2. GABA and glutamate in PCP gray and white matter

By applying MRSI for assessing tissue-type specific metabolite measures, significantly higher levels of both GABA and Glutamate resulted for gray matter compared to white matter (GABA, gray matter: mean ± SD: 0.42 ± 0.27; GABA, white matter: 0.3 ± 0.17; $t(45) = 2.26$, $p = 0.03$; Glutamate, gray matter: mean ± SD: 1.32 ± 0.5; Glutamate, white matter: 0.84 ± 0.26; $t(50) = 4.24$, $p = 0.0001$). Subsequent analyses used only gray matter measures of GABA and glutamate, as brain activity and beta-amyloid were exclusively measured in gray matter and previous work indicated that MRSI metabolite changes in PCP gray matter are more relevant compared to PCP white matter in a context of aging, cognition, and beta-amyloid (Schreiner et al., 2018).
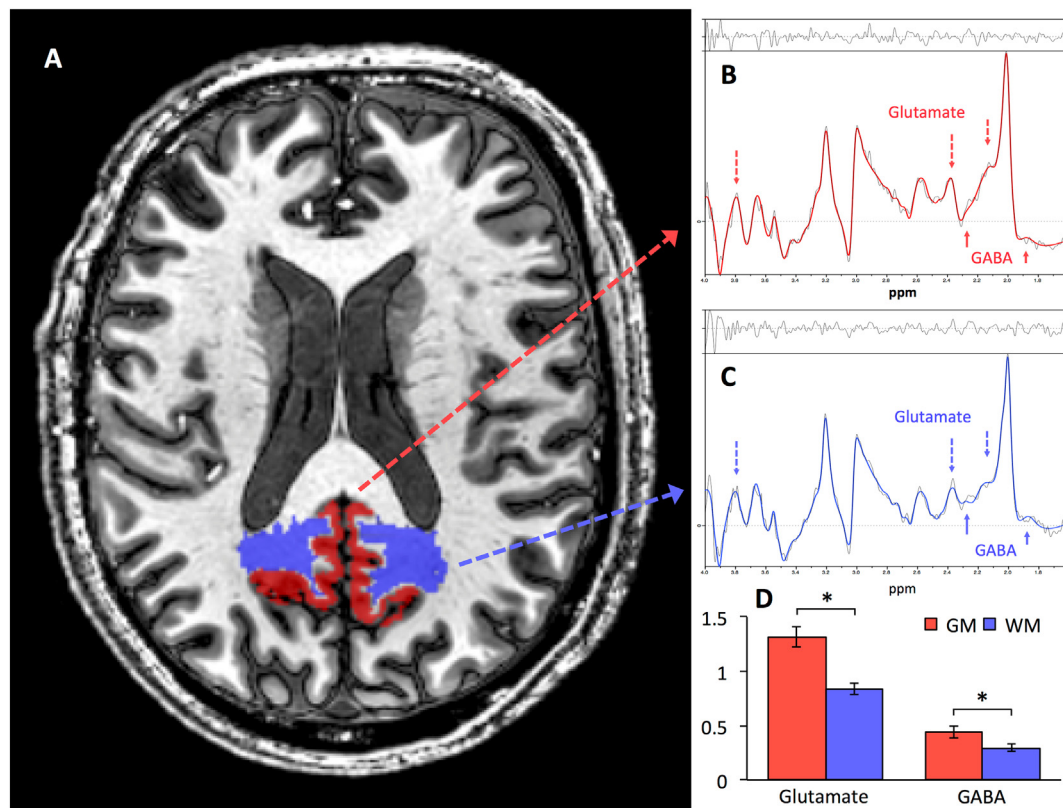
Fig. 2. Measuring Regional Gray and White Matter Levels of GABA and Glutamate with Tissue-specific MRSI at 7 T.

3.3. Beta-amyloid, GABA and glutamate alter static PCP connectivity

Static PCP functional connectivity according to global beta-amyloid load and GABA and glutamate levels in PCP gray matter were assessed using the CONN toolbox. Cortical beta-amyloid load was inferred from PiB measures, thus the term beta-amyloid will be used forthwith instead of PiB for clarity.

Relationships between cortical beta-amyloid and PCP connectivity was observable for 10 clusters (6 clusters with negative connectivity). Positively connected clusters primarily included the Lingual Gyrus, the left Temporal Fusiform Cortex (posterior division), left Lateral Occipital Cortex, the left Inferior Temporal Gyrus, the left posterior Middle Temporal Gyrus, the anterior Parahippocampal Gyrus, the Hippocampus, the Putamen, Thalamus, the Amygdala, the left Temporal Pole, and the right Occipital Fusiform Gyrus. Regions with negative PCP connectivity included the Frontomedial Cortex, the Subcallosal cortex, the Frontal Orbital Cortex, the right posterior Inferior Temporal Gyrus, the right posterior Middle Temporal Gyrus, and the left posterior Parahippocampal Gyrus (Fig. 3).

Rendered 3D brains and coronal brain slices showing regions with increased (red) connectivity and decreased (blue) PCP connectivity associated with global cortical beta-amyloid load. Cluster thresholds for visualization of these clusters were different from the analysis with a cluster threshold of $p < 0.05$ (FDR-corrected). (For interpretation of the references to color in this figure legend, the reader is referred to the web version of this article.)

The interaction of GABA and beta-amyloid affected a wider array of regions (18 clusters), with positively associated clusters covering frontomedial regions, such as Middle Frontal Gyrus, the left Superior Frontal Gyrus, the right Frontal Orbital Cortex, the right Frontal Pole, the Precuneus, the Inferior Frontal Gyrus pars triangularis and the Paracingulate Gyrus and some cerebellar regions. Clusters with negative PCP connectivity mainly include occipital regions, such as the Occipital Fusiform Gyrus and the left Occipital Pole (Fig. 4A).

The glutamate and beta-amyloid interaction displayed a different array of altered PCP functional connectivity networks (9 clusters). Positive PCP connectivity were in clusters covering regions of the Cerebellum, the Middle Frontal Gyrus, the right Superior Frontal Gyrus, and the Inferior Frontal Gyrus pars opercularis and similar to GABA, negatively connected clusters covered occipital areas, including the left and right Occipital Fusiform Gyrus, the left and right Lingual Gyrus, the Lateral Occipital Cortex, and the right Temporal Occipital Fusiform Cortex (Fig. 4B).

Rendered 3D brains and coronal brain slices showing regions with increased (red) connectivity and decreased (blue) PCP connectivity associated with (A) GABA interacting with global beta-amyloid, (B) Glutamate interacting with beta-amyloid. Cluster thresholds for visualization of these clusters were different from the analysis with a voxel height threshold of $p < 0.02$ (uncorrected) and a cluster threshold of $p < 0.05$ (FDR-corrected). (For interpretation of the references to color in this figure legend, the reader is referred to the web version of this article.)

3.4. Dynamic connectivity: Effect of GABA and glutamate and global Beta-amyloid on functional connectivity

No significant correlations were found between the percentage of positive weights and GABA or with glutamate (Table 2). Moreover, global beta-amyloid did not have any significant correlations with eigenconnectivity weights (Table 3).

3.5. GABA and regional Beta-amyloid relate to dynamic functional connectivity

To explore interactive effects of GABA and glutamate on beta-amyloid networks on a multivariate level, CCA was used. By applying CCA, we explored possible relationships indicated by canonical functions, representing linear combinations of maximal correlation between
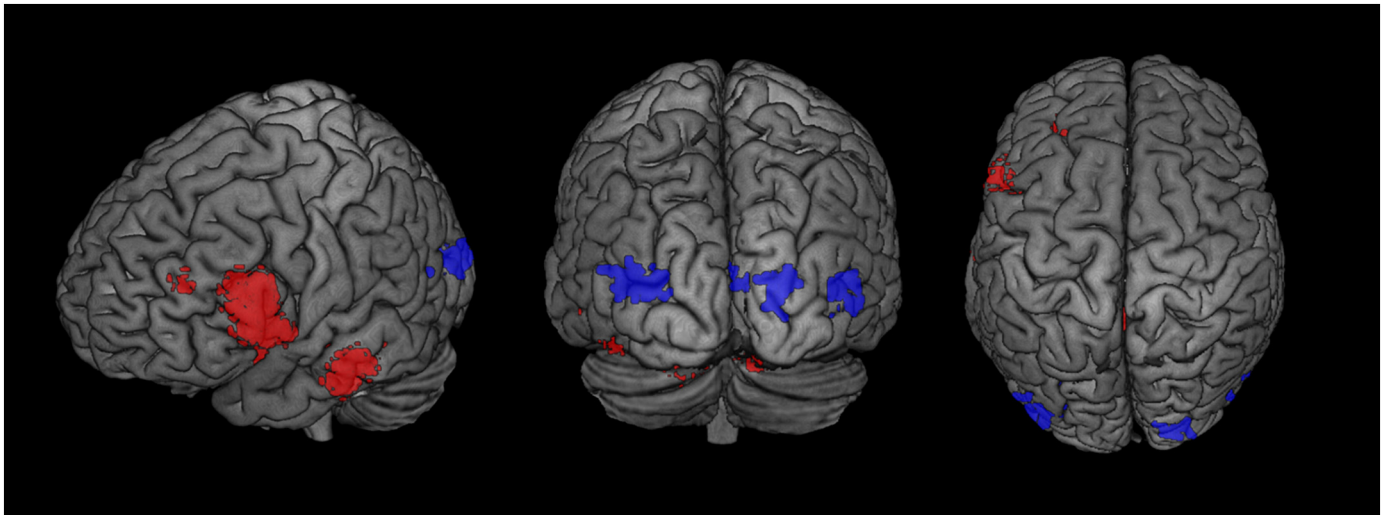
Fig. 3. Beta-amyloid Load Relates to Changes in Static Functional Connectivity.

compared variable sets.

No significant interactive effects on the percentage of positive weights with local beta-amyloid deposition and glutamate were observable. However, CCA indicated a significant difference in the amount of time the eigenconnectivities spent in a positive configuration in subjects with regional beta-amyloid in the Amygdala ($F(2,21) = 3.51$, $p\text{-}FDR = 0.048$), Frontal lobe ($F(2,21) = 3.57$, $p\text{-}FDR = 0.046$), Hippocampus ($F(2,21) = 3.66$, $p\text{-}FDR = 0.04$), Insula ($F(2,21) = 3.53$, $p = 0.048$) and Striatum ($F(2,21) = 3.74$, $p\text{-}FDR = 0.04$)

interacting with PCP GABA.

Furthermore, factor cross-loadings derived from CCA indicated that the first network (eigenconnectivity), which captures global-signal fluctuations, is most strongly altered according to regional beta-amyloid and PCP GABA load ($r = -0.496$) (Fig. 5A). The negative sign suggested apreference for globally decreased connectivity over time, related to GABA and beta-amyloid levels. Moreover, strong effect sizes were found for a fronto-occipital network ($r = 0.27$) (Fig. 5B) and a temporo-parietal network ($r = 0.27$) (Fig. 4C), which both showed
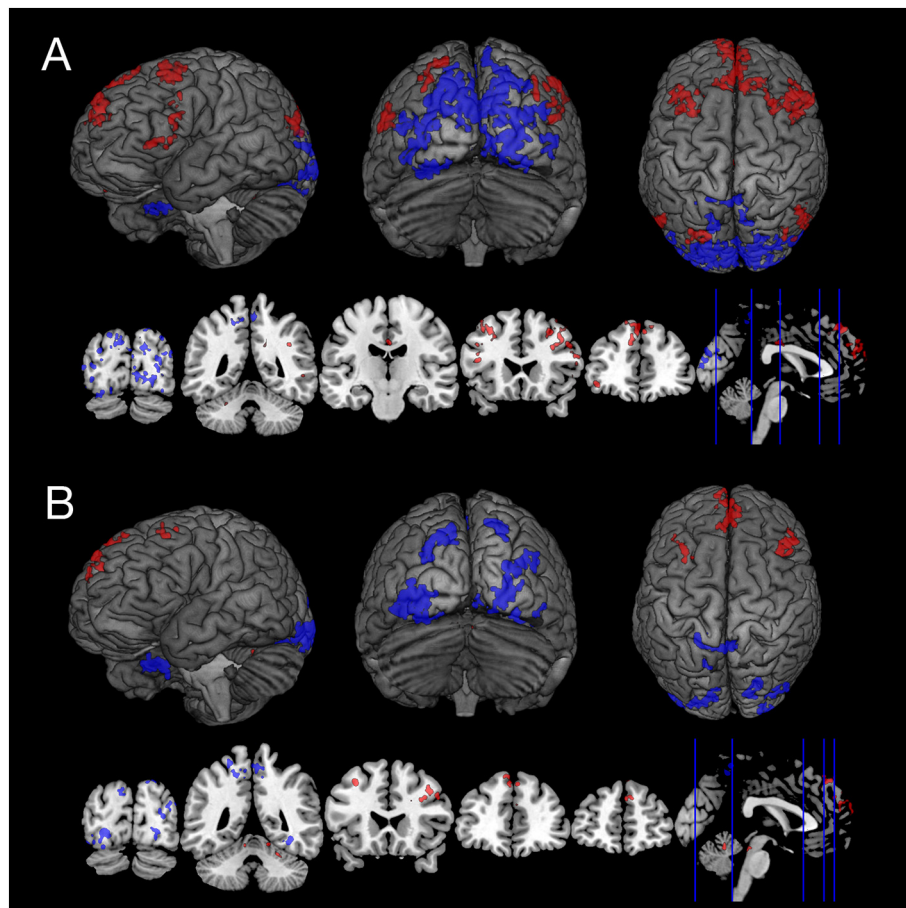

Fig. 4. Beta-amyloid Load Interacts with Gray Matter GABA and Glutamate on Static Functional Connectivity Networks.

Table 2
Correlations between the percentage of positive weights of each eigenconnectivity and GABA and Glutamate measures in the PCP gray matter.

	Eigenconnectivity	r-value	p-FDR		Eigenconnectivity	r-value	p-FDR
GABA	1	0.09	0.74	Glutamate	1	0.21	0.94
	2	−0.42	0.41		2	0.17	0.96
	3	−0.24	0.5		3	0.03	0.95
	4	−0.17	0.73		4	−0.08	0.92
	5	0.15	0.68		5	0.04	0.84
	6	−0.41	0.25		6	−0.02	0.9
	7	0.34	0.36		7	−0.14	1.08
	8	0.27	0.45		8	−0.22	1.05
	9	0.13	0.67		9	−0.19	0.92
	10	−0.002	0.99		10	0.12	1.08

Table 3
Correlations between the percentage of positive weights of each eigenconnectivity and cortical global beta-amyloid load.

	Eigenconnectivity	r-value	p-FDR
Global ß-amyloid	1	−0.36	0.27
	2	−0.42	0.23
	3	−0.25	0.4
	4	−0.36	0.18
	5	−0.12	0.91
	6	0.04	0.93
	7	0.3	0.28
	8	−0.11	0.81
	9	0.002	0.99
	10	0.07	0.89

occipital network and row C a temporo-parietal network. From left to right: Far left is the eigenconnectivity plots wherein the x- and y-axes represent a regions corresponding to the AAL atlas. Red indicates 'positive' connections and blue indicates 'negative' connections. Alongside, glass brains show the axial, sagittal and coronal views of the 2% strongest connections in each network. Brain regions are illustrated as spherical nodes where the size denotes their degree and their color symbolizes the algebraic sign of the relative node strength (red/yellow for positive, blue/green for negative). The same color scheme is applied for the connections. The scatter plots on the far right depict the relationship between the percentage of positive weights (y-axis) and the first canonical of GABA*beta-amyloid (x-axis) with corresponding r-values to show the strength of this relationship. (For interpretation of the references to color in this figure legend, the reader is referred to the web version of this article.)
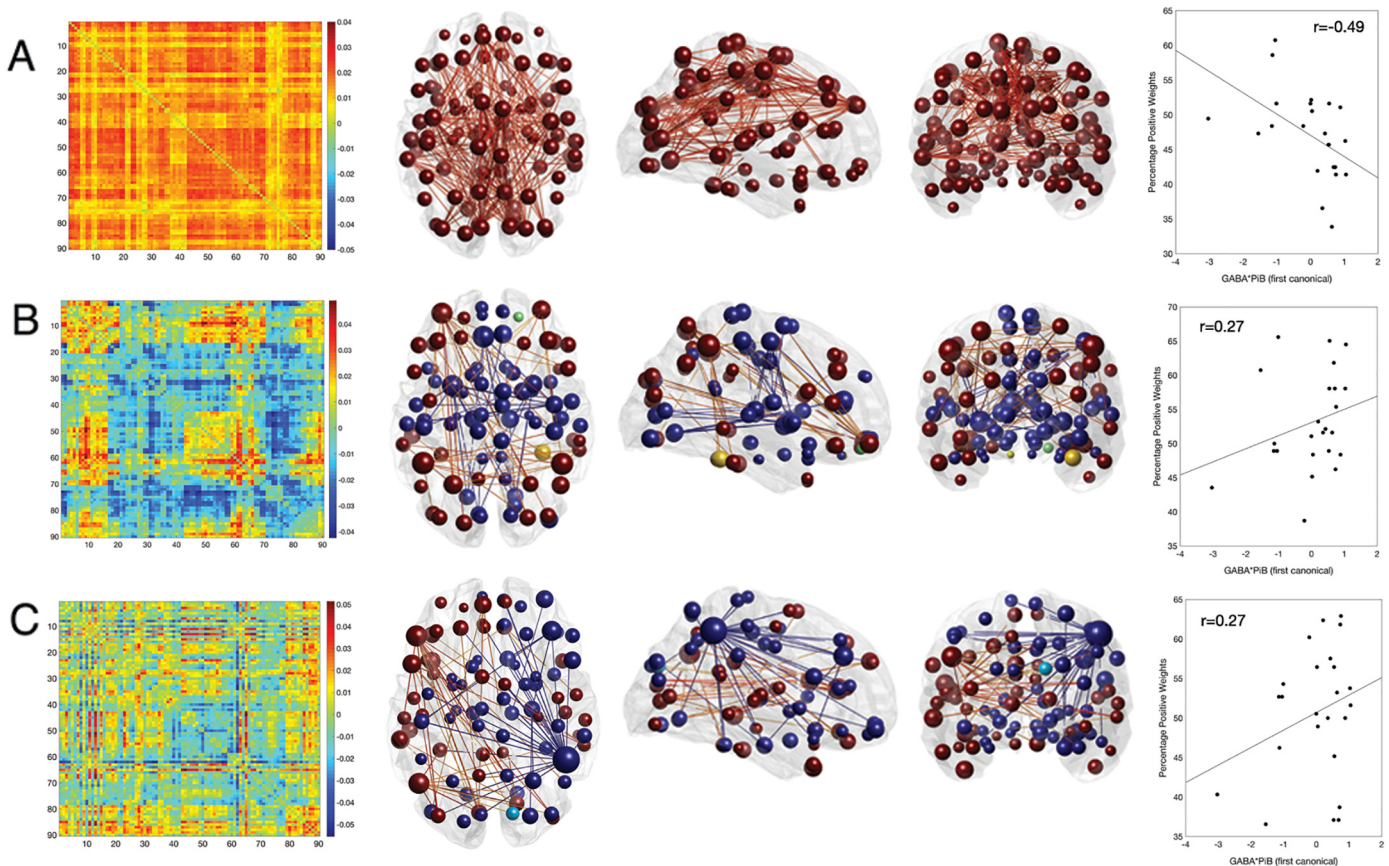
preferences for the positive configuration over time, indicating positive connectivity between involved nodes.

From A-C: Row A illustrates a global network, row B a fronto-

Fig. 5. Beta-amyloid Load Interacts with Gray Matter GABA, but not Glutamate, on Dynamic Functional Connectivity Networks.

4. Discussion

In this cognitively unimpaired old-aged sample, beta-amyloid was associated with altered PCP connectivity in several clusters, including the frontal, inferior temporal and occipital regions. These beta-amyloid-related connectivity changes were moderated by both GABA and glutamate. Though the interaction between beta-amyloid and glutamate affected PCP connectivity in a different cluster array, obtained data indicate that connectivity changes associated with the interaction between beta-amyloid and GABA may be more prominent in both static and dynamic connectivity networks. Interactive static connectivity changes observed with GABA and beta-amyloid, and also glutamate and beta-amyloid, showed increases in PCP connectivity primarily in frontomedial regions and decreased PCP connectivity in clusters located mainly in occipital regions. However, changes to dynamic connectivity were only found for the interaction of GABA with regional beta-amyloid deposits in the Amygdala, Frontal Lobe, Hippocampus, Insula and Striatum, which affected the percentage of positive weights of a global, a fronto-occipital, and a temporo-parietal network. While GABA and regional beta-amyloid interactions showed decreased global connectivity, fronto-occipital and temporo-parietal connections indicated a preference for increased connectivity.

By applying a previously established approach for performing MRSI in clinical study populations (Schreiner et al., 2018), PCP glutamate and GABA were assessed specifically for gray and white matter. This approach included post-processing, i.e. ROI-definition and tissue-segmentation, with state-of-the-art acquisition methods that reduce limitations and exploit benefits of the ultra high magnetic field strength achieved at 7 T, including increased signal to noise ratio and high spatial resolution (Bogner et al., 2012; Fillmer et al., 2015; Henning et al., 2009; Kirchner et al., 2015). BOLD fMRI resting state data was investigated using both static and dynamic approaches to provide refined information on intrinsic brain network activity. To this effect established approaches were used for investigating synchronicity of BOLD signal in spatially distinct brain regions for static connectivity (Friston et al., 1993), and also a sliding window approach for assessing temporal dynamics of brain networks (Chao-Gan and Yu-Feng, 2010; Preti et al., 2017; Quevenco et al., 2017a; Richiardi et al., 2012).

Our data indicate higher PCP levels of GABA and glutamate in gray compared to white matter. These findings are in agreement with earlier reports for other cortical regions and physiological distribution of neurotransmitters (Goryawala et al., 2016; Jensen et al., 2005). Our finding of GABA and glutamate-related functional connectivity accords with earlier 3 T single-voxel MR spectroscopy studies (Ghisleni et al., 2015; Michels et al., 2012; Muthukumaraswamy et al., 2009; Northoff et al., 2007). Moreover, preclinical studies using two-photon Ca2 + imaging in mice showed that despite a net reduction in cortical neuronal activity, many neurons near beta-amyloid plaques were *'hyperactive'* (Busche et al., 2008). Interestingly, the amyloid precursor protein and its cleavage product beta-amyloid 1–42 have been demonstrated to interfere with GABAergic transmission (Rice et al., 2019; Ulrich, 2015). The Clinical evidence on excitatory and inhibitory neurotransmission in AD is less accurate, as measuring GABA and glutamate with neuroimaging is technically challenging. Brain glutamate and GABA levels have been demonstrated to be changed in AD (Bai et al., 2015; Rupsingh et al., 2011) and furthermore linked to altered brain activity in non-demented adults (Ghisleni et al., 2015; Michels et al., 2012; Muthukumaraswamy et al., 2009).

Also, consistent with earlier reports, we find changes in connectivity associated with beta-amyloid deposits prior to signs of cognitive decline or other AD-related symptoms (Sheline et al., 2010; Sperling et al., 2009). Furthermore, a prominent observation in previous literature is increased connectivity with frontal brain regions, which is thought to indicate compensatory changes (Agosta et al., 2012; Gould et al., 2006; Supekar et al., 2008; Wang et al., 2007; Franzmeier et al., 2018; Hahn et al., 2019). This coincides with our finding of GABA and glutamate interacting with global beta-amyloid and PCP connectivity in frontal regions of the brain. We only found dynamic functional connectivity changes for the interaction between GABA and beta-amyloid load. These were specifically localized to regions intimately linked to the DMN and affected in early stages of AD (Sperling et al., 2009). Our finding of globally decreased connectivity and at the same time selectively increased connectivity between fronto-occipital and temporo-parietal nodes may appear counterintuitive at first glance. However, local 'high efficiency' (hyperconnectivity) in brain regions with long anatomical connections might represent a dynamic strategy to minimise metabolic costs (Zalesky et al., 2014).

Prior studies have highlighted a relationship between neuronal excitation and beta-amyloid (Cirrito et al., 2008; Cirrito et al., 2005; Kamenetz et al., 2003; Nitsch et al., 1993; Palop et al., 2007). Thus, we expected to see major impacts of glutamate on functional connectivity, when interacting with beta-amyloid, considering its role as a major excitatory neurotransmitter and its implication in long-term potentiation (LTP). However, while our findings suggest stronger effects for the interaction between GABA and beta-amyloid, follow-up studies are needed to confirm our findings. Moreover, by better characterizing the natural history of GABA and beta-amyloid interactions during the course of AD, promise of the GABAergic system as a target for pharmacological intervention may be validated (Calvo-Flores Guzman et al., 2018).

Although this study provides novel findings and has strengths such as the unique combination of advanced neuroimaging methods, there are limitations that need to be taken into consideration. Due to the long acquisition time of ca. 29 min for completing the FIDLOVS MRSI for one brain region located in the PCP, only a relatively small sized population of cognitively healthy old aged adults could be investigated. For increased power, subsequent studies might use lower spatial MRSI resolution, allowing for a shorter MRSI sequence and larger populations that include cognitively impaired participants. Also, when using lower resolution MRSI sequences, follow-up studies might investigate additional brain regions with high susceptibility to AD pathology, such as the medio-temporal and parietal cortex. Alternatively, the development of novel, innovative PET tracers might provide the means for investigating regional variation of neurotransmitters in AD (Lin et al., 2017; van der Aart et al., 2018). Moreover, while the ultra-high magnetic field strength applied in the current study enabled tissue specific estimation of GABA (and glutamate), due to the lack of spectral editing in our MRSI approach, some overlap between spectral peaks of GABA with other metabolites and macromolecules is to be expected. This imprecision for estimation of GABA is a limitation of our study, which is why careful interpretation and replication of our findings are warranted. Another limitation is the cross-sectional nature of this study. To fully investigate whether the effects of GABA and glutamate in conjunction with beta-amyloid deposits on functional connectivity are more likely pathological in nature or compensatory, it would be ideal to follow-up with a longitudinal study including individuals that vary in progression of AD pathology.

In conclusion, this study confirms earlier non-human studies by providing first evidence of a moderating relationship between GABA and to a lesser degree also glutamate on beta-amyloid related functional brain networks in cognitively unimpaired old-aged humans. Moreover, to our knowledge, this study is the first attempt to implement non-invasive neuroimaging techniques to assess relationships between GABA, glutamate and beta-amyloid on functional connectivity. Additional longitudinal studies are needed to determine how progression of AD may relate to GABA and glutamate levels, and thus exploit novel possibilities for neurotransmitter targeted therapeutic intervention.

Declarations of interest

None.

Acknowledgements

References

Agosta, F., Pievani, M., Geroldi, C., Copetti, M., Frisoni, G.B., Filippi, M., 2012. Resting state fMRI in Alzheimer's disease: beyond the default mode network. Neurobiol. Aging 33, 1564–1578.

Albert, M.S., DeKosky, S.T., Dickson, D., Dubois, B., Feldman, H.H., Fox, N.C., Gamst, A., Holtzman, D.M., Jagust, W.J., Petersen, R.C., Snyder, P.J., Carrillo, M.C., Thies, B., Phelps, C.H., 2011. The diagnosis of mild cognitive impairment due to Alzheimer's disease: recommendations from the National Institute on Aging-Alzheimer's Association workgroups on diagnostic guidelines for Alzheimer's disease. Alzheimers Dement. 7, 270–279.

Allen, E.A., Damaraju, E., Plis, S.M., Erhardt, E.B., Eichele, T., Calhoun, V.D., 2014. Tracking whole-brain connectivity dynamics in the resting state. Cereb. Cortex 24, 663–676.

Bai, X., Edden, R.A., Gao, F., Wang, G., Wu, L., Zhao, B., Wang, M., Chan, Q., Chen, W., Barker, P.B., 2015. Decreased gamma-aminobutyric acid levels in the parietal region of patients with Alzheimer's disease. J. Magn. Reson. Imaging 41, 1326–1331.

Benjamini, Y., Hochberg, Y., 1995. Controlling the false discovery rate: a practical and powerful approach to multiple testing. J. R. Stat. Soc. Ser. B 57, 289–300.

Bero, A.W., Yan, P., Roh, J.H., Cirrito, J.R., Stewart, F.R., Raichle, M.E., Lee, J.M., Holtzman, D.M., 2011. Neuronal activity regulates the regional vulnerability to amyloid-beta deposition. Nat. Neurosci. 14, 750–756.

Bogner, W., Gruber, S., Trattnig, S., Chmelik, M., 2012. High-resolution mapping of human brain metabolites by free induction decay (1)H MRSI at 7 T. NMR Biomed. 25, 873–882.

Brettschneider, J., Del Tredici, K., Lee, V.M., Trojanowski, J.Q., 2015. Spreading of pathology in neurodegenerative diseases: a focus on human studies. Nat. Rev. Neurosci. 16, 109–120.

Buckner, R.L., Andrews-Hanna, J.R., Schacter, D.L., 2008. The brain's default network: anatomy, function, and relevance to disease. Ann. N. Y. Acad. Sci. 1124, 1–38.

Buckner, R.L., Sepulcre, J., Talukdar, T., Krienen, F.M., Liu, H., Hedden, T., Andrews-Hanna, J.R., Sperling, R.A., Johnson, K.A., 2009. Cortical hubs revealed by intrinsic functional connectivity: mapping, assessment of stability, and relation to Alzheimer's disease. J. Neurosci. 29, 1860–1873.

Busche, M.A., Eichhoff, G., Adelsberger, H., Abramowski, D., Wiederhold, K.H., Haass, C., Staufenbiel, M., Konnerth, A., Garaschuk, O., 2008. Clusters of hyperactive neurons near amyloid plaques in a mouse model of Alzheimer's disease. Science 321, 1686–1689.

Calvo-Flores Guzman, B., Vinnakota, C., Govindpani, K., Waldvogel, H.J., Faull, R.L.M., Kwakowsky, A., 2018. The GABAergic system as a therapeutic target for Alzheimer's disease. J. Neurochem. 146, 649–669.

Chang, C., Glover, G.H., 2010. Time-frequency dynamics of resting-state brain connectivity measured with fMRI. Neuroimage 50, 81–98.

Chao-Gan, Y., Yu-Feng, Z., 2010. DPARSF: a MATLAB toolbox for "Pipeline" data analysis of resting-state fMRI. Front. Syst. Neurosci. 4, 13.

Cieri, F., Esposito, R., 2018. Neuroaging through the Lens of the resting state networks. Biomed. Res. Int. 2018, 5080981.

Cirrito, J.R., Yamada, K.A., Finn, M.B., Sloviter, R.S., Bales, K.R., May, P.C., Schoepp, D.D., Paul, S.M., Mennerick, S., Holtzman, D.M., 2005. Synaptic activity regulates interstitial fluid amyloid-beta levels in vivo. Neuron 48, 913–922.

Cirrito, J.R., Kang, J.E., Lee, J., Stewart, F.R., Verges, D.K., Silverio, L.M., Bu, G., Mennerick, S., Holtzman, D.M., 2008. Endocytosis is required for synaptic activity-dependent release of amyloid-beta in vivo. Neuron 58, 42–51.

Corder, E.H., Saunders, A.M., Strittmatter, W.J., Schmechel, D.E., Gaskell, P.C., Small, G.W., Roses, A.D., Haines, J.L., Pericak-Vance, M.A., 1993. Gene dose of apolipoprotein E type 4 allele and the risk of Alzheimer's disease in late onset families. Science 261, 921–923.

Dubois, B., Hampel, H., Feldman, H.H., Scheltens, P., Aisen, P., Andrieu, S., Bakardjian, H., Benali, H., Bertram, L., Blennow, K., Broich, K., Cavedo, E., Crutch, S., Dartigues, J.F., Duyckaerts, C., Epelbaum, S., Frisoni, G.B., Gauthier, S., Genthon, R., Gouw, A.A., Habert, M.O., Holtzman, D.M., Kivipelto, M., Lista, S., Molinuevo, J.L., O'Bryant, S.E., Rabinovici, G.D., Rowe, C., Salloway, S., Schneider, L.S., Sperling, R., Teichmann, M., Carrillo, M.C., Cummings, J., Jack, C.R., Proceedings of the Meeting of the International Working, G., the American Alzheimer's Association on "The Preclinical State of, A.D., July, Washington Dc, U.S.A, 2016. Preclinical Alzheimer's disease: definition, natural history, and diagnostic criteria. Alzheimers Dement. 12, 292–323.

Esposito, R., Mosca, A., Pieramico, V., Cieri, F., Cera, N., Sensi, S.L., 2013. Characterization of resting state activity in MCI individuals. PeerJ 1, e135.

Ferreira, L.K., Busatto, G.F., 2013. Resting-state functional connectivity in normal brain aging. Neurosci. Biobehav. Rev. 37, 384–400.

Fillmer, A., Kirchner, T., Cameron, D., Henning, A., 2015. Constrained image-based B0 shimming accounting for "local minimum traps" in the optimization and field inhomogeneities outside the region of interest. Magn. Reson. Med. 73, 1370–1380.

Folstein, M.F., Folstein, S.E., McHugh, P.R., 1975. Mini-mental state: A practical method for grading the cognitive state of patients for the clinician. J. Psychiatr. Res. 12, 189–198.

Fox, M.D., Raichle, M.E., 2007. Spontaneous fluctuations in brain activity observed with functional magnetic resonance imaging. Nat. Rev. Neurosci. 8, 700–711.

Franzmeier, N., Duering, M., Weiner, M., Dichgans, M., Ewers, M., Alzheimer's Disease Neuroimaging, I., 2017. Left frontal cortex connectivity underlies cognitive reserve in prodromal Alzheimer disease. Neurology 88, 1054–1061.

Franzmeier, N., Hartmann, J., Taylor, A.N.W., Araque-Caballero, M.A., Simon-Vermot, L., Kambeitz-Ilankovic, L., Burger, K., Catak, C., Janowitz, D., Muller, C., Ertl-Wagner, B., Stahl, R., Dichgans, M., Duering, M., Ewers, M., 2018. The left frontal cortex supports reserve in aging by enhancing functional network efficiency. Alzheimers Res. Ther. 10, 28.

Friston, K.J., Frith, C.D., Liddle, P.F., Frackowiak, R.S., 1993. Functional connectivity: the principal-component analysis of large (PET) data sets. J. Cereb. Blood Flow Metab. 13, 5–14.

Ghisleni, C., Bollmann, S., Poil, S.S., Brandeis, D., Martin, E., Michels, L., O'Gorman, R.L., Klaver, P., 2015. Subcortical glutamate mediates the reduction of short-range functional connectivity with age in a developmental cohort. J. Neurosci. 35, 8433–8441.

Gietl, A.F., Warnock, G., Riese, F., Kalin, A.M., Saake, A., Gruber, E., Leh, S.E., Unschuld, P.G., Kuhn, F.P., Burger, C., Mu, L., Seifert, B., Nitsch, R.M., Schibli, R., Ametamey, S.M., Buck, A., Hock, C., 2015. Regional cerebral blood flow estimated by early PiB uptake is reduced in mild cognitive impairment and associated with age in an amyloid-dependent manner. Neurobiol. Aging 36, 1619–1628.

Goryawala, M.Z., Sheriff, S., Maudsley, A.A., 2016. Regional distributions of brain glutamate and glutamine in normal subjects. NMR Biomed. 29, 1108–1116.

Gould, R.L., Arroyo, B., Brown, R.G., Owen, A.M., Bullmore, E.T., Howard, R.J., 2006. Brain mechanisms of successful compensation during learning in Alzheimer disease. Neurology 67, 1011–1017.

Gousias, I.S., Rueckert, D., Heckemann, R.A., Dyet, L.E., Boardman, J.P., Edwards, A.D., Hammers, A., 2008. Automatic segmentation of brain MRIs of 2-year-olds into 83 regions of interest. Neuroimage 40, 672–684.

Gregoire, J., Van der Linden, M., 1997. Effect of age on forward and backward digit spans. Aging Neuropsychol. Cognit. 4, 140–149.

Greicius, M.D.K., Reiss, A.L., Menon, V., 2003. Functional connectivity in the resting brain: a network analysis of the default mode hypothesis. PNAS 100, 253–258.

Hahn, A., Strandberg, T.O., Stomrud, E., Nilsson, M., van Westen, D., Palmqvist, S., Ossenkoppele, R., Hansson, O., 2019. Association Between Earliest Amyloid Uptake and Functional Connectivity in Cognitively Unimpaired Elderly. Cereb. Cortex.

Hammers, A., Allom, R., Koepp, M.J., Free, S.L., Myers, R., Lemieux, L., Mitchell, T.N., Brooks, D.J., Duncan, J.S., 2003. Three-dimensional maximum probability atlas of the human brain, with particular reference to the temporal lobe. Hum. Brain Mapp. 19, 224–247.

Handwerker, D.A., Roopchansingh, V., Gonzalez-Castillo, J., Bandettini, P.A., 2012. Periodic changes in fMRI connectivity. Neuroimage 63, 1712–1719.

Hedden, T., Van Dijk, K.R., Becker, J.A., Mehta, A., Sperling, R.A., Johnson, K.A., Buckner, R.L., 2009. Disruption of functional connectivity in clinically normal older adults harboring amyloid burden. J. Neurosci. 29, 12686–12694.

Henning, A., Fuchs, A., Murdoch, J.B., Boesiger, P., 2009. Slice-selective FID acquisition, localized by outer volume suppression (FIDLOVS) for (1)H-MRSI of the human brain at 7 T with minimal signal loss. NMR Biomed. 22, 683–696.

Hutchison, R.M., Womelsdorf, T., Allen, E.A., Bandettini, P.A., Calhoun, V.D., Corbetta, M., Della Penna, S., Duyn, J.H., Glover, G.H., Gonzalez-Castillo, J., Handwerker, D.A., Keilholz, S., Kiviniemi, V., Leopold, D.A., de Pasquale, F., Sporns, O., Walter, M., Chang, C., 2013. Dynamic functional connectivity: promise, issues, and interpretations. Neuroimage 80, 360–378.

Jack Jr., C.R., Lowe, V.J., Weigand, S.D., Wiste, H.J., Senjem, M.L., Knopman, D.S., Shiung, M.M., Gunter, J.L., Boeve, B.F., Kemp, B.J., Weiner, M., Petersen, R.C., Alzheimer's Disease Neuroimaging, I, 2009. Serial PIB and MRI in normal, mild cognitive impairment and Alzheimer's disease: implications for sequence of pathological events in Alzheimer's disease. Brain 132, 1355–1365.

Jagust, W.J., Mormino, E.C., 2011. Lifespan brain activity, beta-amyloid, and Alzheimer's disease. Trends Cogn. Sci. 15, 520–526.

Jensen, J.E., Frederick Bde, B., Renshaw, P.F., 2005. Grey and white matter GABA level differences in the human brain using two-dimensional, J-resolved spectroscopic imaging. NMR Biomed. 18, 570–576.

Kamenetz, F., Tomita, T., Hsieh, H., Seabrook, G., Borchelt, D., Iwatsubo, T., Sisodia, S., Malinow, R., 2003. APP processing and synaptic function. Neuron 37, 925–937.

Kantarci, K., Lowe, V., Przybelski, S.A., Weigand, S.D., Senjem, M.L., Ivnik, R.J., Preboske, G.M., Roberts, R., Geda, Y.E., Boeve, B.F., Knopman, D.S., Petersen, R.C., Jack Jr., C.R., 2012. APOE modifies the association between Abeta load and cognition in cognitively normal older adults. Neurology 78, 232–240.

Kirchner, T., Fillmer, A., Tsao, J., Pruessmann, K.P., Henning, A., 2015. Reduction of voxel bleeding in highly accelerated parallel (1) H MRSI by direct control of the spatial response function. Magn. Reson. Med. 73, 469–480.

Klunk, W.E., Engler, H., Nordberg, A., Wang, Y., Blomqvist, G., Holt, D.P., Bergstrom, M., Savitcheva, I., Huang, G.F., Estrada, S., Ausen, B., Debnath, M.L., Barletta, J., Price,

J.C., Sandell, J., Lopresti, B.J., Wall, A., Koivisto, P., Antoni, G., Mathis, C.A., Langstrom, B., 2004. Imaging brain amyloid in Alzheimer's disease with Pittsburgh Compound-B. Ann. Neurol. 55, 306–319.

Kreis, R., 2016. The trouble with quality filtering based on relative Cramer-Rao lower bounds. Magn. Reson. Med. 75, 15–18.

Lange, K.L., Bondi, M.W., Salmon, D.P., Galasko, D., Delis, D.C., Thomas, R.G., Thal, L.J., 2002. Decline in verbal memory during preclinical Alzheimer's disease: examination of the effect of APOE genotype. J. Int. Neuropsychol. Soc. 8, 943–955.

Leonardi, N., Richiardi, J., Gschwind, M., Simioni, S., Annoni, J.M., Schluep, M., Vuilleumier, P., Van De Ville, D., 2013. Principal components of functional connectivity: a new approach to study dynamic brain connectivity during rest. Neuroimage 83, 937–950.

Lin, S.F., Bois, F., Holden, D., Nabulsi, N., Pracitto, R., Gao, H., Kapinos, M., Teng, J.K., Shirali, A., Ropchan, J., Carson, R.E., Elmore, C.S., Vasdev, N., Huang, Y., 2017. The search for a subtype-selective PET imaging agent for the GABAA receptor complex: evaluation of the radiotracer [(11)C]ADO in nonhuman primates. Mol. Imaging 16, 1536012117731258.

Lustig, C., Snyder, A.Z., Bhakta, M., O'Brien, K.C., McAvoy, M., Raichle, M.E., Morris, J.C., Buckner, R.L., 2003. Functional deactivations: change with age and dementia of the Alzheimer type. Proc. Natl. Acad. Sci. U. S. A. 100, 14504–14509.

Michels, L., Martin, E., Klaver, P., Edden, R., Zelaya, F., Lythgoe, D.J., Luchinger, R., Brandeis, D., O'Gorman, R.L., 2012. Frontal GABA levels change during working memory. PLoS One 7, e31933.

Mormino, E.C., Smiljic, A., Hayenga, A.O., Onami, S.H., Greicius, M.D., Rabinovici, G.D., Janabi, M., Baker, S.L., Yen, I.V., Madison, C.M., Miller, B.L., Jagust, W.J., 2011. Relationships between beta-amyloid and functional connectivity in different components of the default mode network in aging. Cereb. Cortex 21, 2399–2407.

Muthukumaraswamy, S.D.E, R.A., Jones, D.K., Swettenham, J.B., Singh, K.D., 2009. Resting GABA concentration predicts peak gamma frequency and fMRI amplitude in response to visual stimulation in humans. PNAS 106, 8356–8361.

Nicholas, L.E., Brookshire, R.H., Schumacher, J.G., Porrazzo, S.A., 1988. The Boston naming test: revised administration and scoring procedures and normative information for non-brain-damaged adults. Clin. Aphasiol. 18, 103–115.

Nitsch, R.M., Farber, S.A., Growden, J.H., Wurtman, R.J., 1993. Release of amyloid ß-protein precursor derivatives by electrical depolarization of rat hipocampal slices. Proc. Natl. Acad. Sci. U. S. A. 90, 5191–5193.

Northoff, G., Walter, M., Schulte, R.F., Beck, J., Dydak, U., Henning, A., Boeker, H., Grimm, S., Boesiger, P., 2007. GABA concentrations in the human anterior cingulate cortex predict negative BOLD responses in fMRI. Nat. Neurosci. 10, 1515–1517.

Palop, J.J., Chin, J., Roberson, E.D., Wang, J., Thwin, M.T., Bien-Ly, N., Yoo, J., Ho, K.O., Yu, G.Q., Kreitzer, A., Finkbeiner, S., Noebels, J.L., Mucke, L., 2007. Aberrant excitatory neuronal activity and compensatory remodeling of inhibitory hippocampal circuits in mouse models of Alzheimer's disease. Neuron 55, 697–711.

Preti, M.G., Bolton, T.A., Van De Ville, D., 2017. The dynamic functional connectome: state-of-the-art and perspectives. Neuroimage 160, 41–54.

Provencher, S.W., 2001. Automatic quantitation of localized in vivo 1H spectra with LCModel. NMR Biomed. 14, 260–264.

Quevenco, F.C.P., van Bergen, J.M.G., Hua, J., Wyss, M., Xu, Li, Schreiner, S.J., Steininger, S.C., Meyer, R., Meier, I.B., Brickman, A.M., Leh, S.E., Gietl, A.F., Buck, A., Nitsch, R.M., Pruessmann, K.P., van Zijl, P.C.M., Hock, C., Van De Ville, D., Unschuld, P.G., 2017a. Memory performance-related dynamic brain connectivity indicates pathological burden and genetic risk for Alzheimer's disease. Alzheimers Res. Ther. 9.

Quevenco, F.C., Preti, M.G., van Bergen, J.M., Hua, J., Wyss, M., Li, X., Schreiner, S.J., Steininger, S.C., Meyer, R., Meier, I.B., Brickman, A.M., Leh, S.E., Gietl, A.F., Buck, A., Nitsch, R.M., Pruessmann, K.P., van Zijl, P.C., Hock, C., Van De Ville, D., Unschuld, P.G., 2017b. Memory performance-related dynamic brain connectivity indicates pathological burden and genetic risk for Alzheimer's disease. Alzheimers Res. Ther. 9, 24.

Raichle, M.E.M, M, A., Snyder, A.Z., Powers, W.J., Gusnard, D.A., Shulman, G.L., 2001. A default mode of brain function. PNAS 98, 676–682.

Rice, H.C., de Malmazet, D., Schreurs, A., Frere, S., Van Molle, I., Volkov, A.N., Creemers, E., Vertkin, I., Nys, J., Ranaivoson, F.M., Comoletti, D., Savas, J.N., Remaut, H., Balschun, D., Wierda, K.D., Slutsky, I., Farrow, K., De Strooper, B., de Wit, J., 2019. Secreted amyloid-beta precursor protein functions as a GABABR1a ligand to modulate synaptic transmission. Science 363.

Richiardi, J., Gschwind, M., Simioni, S., Annoni, J.M., Greco, B., Hagmann, P., Schluep, M., Vuilleumier, P., Van De Ville, D., 2012. Classifying minimally disabled multiple sclerosis patients from resting state functional connectivity. Neuroimage 62, 2021–2033.

Robinson, J.L., Lee, E.B., Xie, S.X., Rennert, L., Suh, E., Bredenberg, C., Caswell, C., Van Deerlin, V.M., Yan, N., Yousef, A., Hurtig, H.I., Siderowf, A., Grossman, M., McMillan, C.T., Miller, B., Duda, J.E., Irwin, D.J., Wolk, D., Elman, L., McCluskey, L., Chen-Plotkin, A., Weintraub, D., Arnold, S.E., Brettschneider, J., Lee, V.M., Trojanowski, J.Q., 2018. Neurodegenerative disease concomitant proteinopathies are prevalent, age-related and APOE4-associated. Brain 141, 2181–2193.

Rupsingh, R., Borrie, M., Smith, M., Wells, J.L., Bartha, R., 2011. Reduced hippocampal

glutamate in Alzheimer disease. Neurobiol. Aging 32, 802–810.

Schreiner, S.J., Liu, X., Gietl, A.F., Wyss, M., Steininger, S.C., Gruber, E., Treyer, V., Meier, I.B., Kalin, A.M., Leh, S.E., Buck, A., Nitsch, R.M., Pruessmann, K.P., Hock, C., Unschuld, P.G., 2014. Regional Fluid-Attenuated Inversion Recovery (FLAIR) at 7 Tesla correlates with amyloid beta in hippocampus and brainstem of cognitively normal elderly subjects. Front. Aging Neurosci. 6, 240.

Schreiner, S.J., Kirchner, T., Wyss, M., Van Bergen, J.M., Quevenco, F.C., Steininger, S.C., Griffith, E.Y., Meier, I., Michels, L., Gietl, A.F., Leh, S.E., Brickman, A.M., Hock, C., Nitsch, R.M., Pruessmann, K.P., Henning, A., Unschuld, P.G., 2016. Low episodic memory performance in cognitively normal elderly subjects is associated with increased posterior cingulate gray matter N-acetylaspartate: a 1H MRSI study at 7 Tesla. Neurobiol. Aging 48, 195–203.

Schreiner, S.J., Kirchner, T., Narkhede, A., Wyss, M., Van Bergen, J.M.G., Steininger, S.C., Gietl, A., Leh, S.E., Treyer, V., Buck, A., Pruessmann, K.P., Nitsch, R.M., Hock, C., Henning, A., Brickman, A.M., Unschuld, P.G., 2018. Brain amyloid burden and cerebrovascular disease are synergistically associated with neurometabolism in cognitively unimpaired older adults. Neurobiol. Aging 63, 152–161.

Seeley, W.W., 2017. Mapping neurodegenerative Disease onset and progression. Cold Spring Harb. Perspect. Biol. 9.

Sepulcre, J., Sabuncu, M.R., Li, Q., El Fakhri, G., Sperling, R., Johnson, K.A., 2017. Tau and amyloid-beta proteins distinctively associate to functional network changes in the aging brain. Alzheimers Dement. 13, 1261–1269.

Sheline, Y.I., Raichle, M.E., Snyder, A.Z., Morris, J.C., Head, D., Wang, S., Mintun, M.A., 2010. Amyloid plaques disrupt resting state default mode network connectivity in cognitively normal elderly. Biol. Psychiatry 67, 584–587.

Sorg, C., Riedl, V., Muhlau, M., Calhoun, V.D., Eichele, T., Laer, L., Drzezga, A., Forstl, H., Kurz, A., Zimmer, C., Wohlschlager, A.M., 2007. Selective changes of resting-state networks in individuals at risk for Alzheimer's disease. Proc. Natl. Acad. Sci. U. S. A. 104, 18760–18765.

Sperling, R.A., Laviolette, P.S., O'Keefe, K., O'Brien, J., Rentz, D.M., Pihlajamaki, M., Marshall, G., Hyman, B.T., Selkoe, D.J., Hedden, T., Buckner, R.L., Becker, J.A., Johnson, K.A., 2009. Amyloid deposition is associated with impaired default network function in older persons without dementia. Neuron 63, 178–188.

Sperling, R.A., Aisen, P.S., Beckett, L.A., Bennett, D.A., Craft, S., Fagan, A.M., Iwatsubo, T., Jack Jr., C.R., Kaye, J., Montine, T.J., Park, D.C., Reiman, E.M., Rowe, C.C., Siemers, E., Stern, Y., Yaffe, K., Carrillo, M.C., Thies, B., Morrison-Bogorad, M., Wagster, M.V., Phelps, C.H., 2011. Toward defining the preclinical stages of Alzheimer's disease: recommendations from the National Institute on Aging-Alzheimer's Association workgroups on diagnostic guidelines for Alzheimer's disease. Alzheimers Dement. 7, 280–292.

Steininger, S.C., Liu, X., Gietl, A., Wyss, M., Schreiner, S., Gruber, E., Treyer, V., Kalin, A., Leh, S., Buck, A., Nitsch, R.M., Prussmann, K.P., Hock, C., Unschuld, P.G., 2014. Cortical amyloid Beta in cognitively Normal elderly adults is associated with decreased network efficiency within the Cerebro-cerebellar system. Front. Aging Neurosci. 6, 52.

Supekar, K., Menon, V., Rubin, D., Musen, M., Greicius, M.D., 2008. Network analysis of intrinsic functional brain connectivity in Alzheimer's disease. PLoS Comput. Biol. 4, e1000100.

Teipel, S., Grothe, M.J., Alzheimer s Disease Neuroimaging, I, 2016a. Does posterior cingulate hypometabolism result from disconnection or local pathology across preclinical and clinical stages of Alzheimer's disease? Eur. J. Nucl. Med. Mol. Imaging 43, 526–536.

Teipel, S.J., Grothe, M.J., Metzger, C.D., Grimmer, T., Sorg, C., Ewers, M., Franzmeier, N., Meisenzahl, E., Kloppel, S., Borchardt, V., Walter, M., Dyrba, M., 2016b. Robust detection of impaired resting state functional connectivity networks in Alzheimer's Disease using elastic net regularized regression. Front. Aging Neurosci. 8, 318.

Tkac, I., Starcuk, Z., Choi, I.Y., Gruetter, R., 1999. In vivo 1H NMR spectroscopy of rat brain at 1 ms echo time. Magn. Reson. Med. 41, 649–656.

Tombaugh, T., 2004. Trail making test A and B: normative data stratified by age and education. Arch. Clin. Neuropsychol. 19, 203–214.

Ulrich, D., 2015. Amyloid-beta impairs synaptic inhibition via GABA(A) receptor endocytosis. J. Neurosci. 35, 9205–9210.

van den Heuvel, M.P., Mandl, R.C., Kahn, R.S., Hulshoff Pol, H.E., 2009. Functionally linked resting-state networks reflect the underlying structural connectivity architecture of the human brain. Hum. Brain Mapp. 30, 3127–3141.

van der Aart, J., Golla, S.S.V., van der Pluijm, M., Schwarte, L.A., Schuit, R.C., Klein, P.J., Metaxas, A., Windhorst, A.D., Boellaard, R., Lammertsma, A.A., van Berckel, B.N.M., 2018. First in human evaluation of [(18)F]PK-209, a PET ligand for the ion channel binding site of NMDA receptors. EJNMMI Res. 8, 69.

Wang, K., Liang, M., Wang, L., Tian, L., Zhang, X., Li, K., Jiang, T., 2007. Altered functional connectivity in early Alzheimer's disease: a resting-state fMRI study. Hum. Brain Mapp. 28, 967–978.

Whitfield-Gabrieli, S., Nieto-Castanon, A., 2012. Conn: a functional connectivity toolbox for correlated and anticorrelated brain networks. Brain Connect 2, 125–141.

Zalesky, A., Fornito, A., Cocchi, L., Gollo, L.L., Breakspear, M., 2014. Time-resolved resting-state brain networks. Proc. Natl. Acad. Sci. U. S. A. 111, 10341–10346.